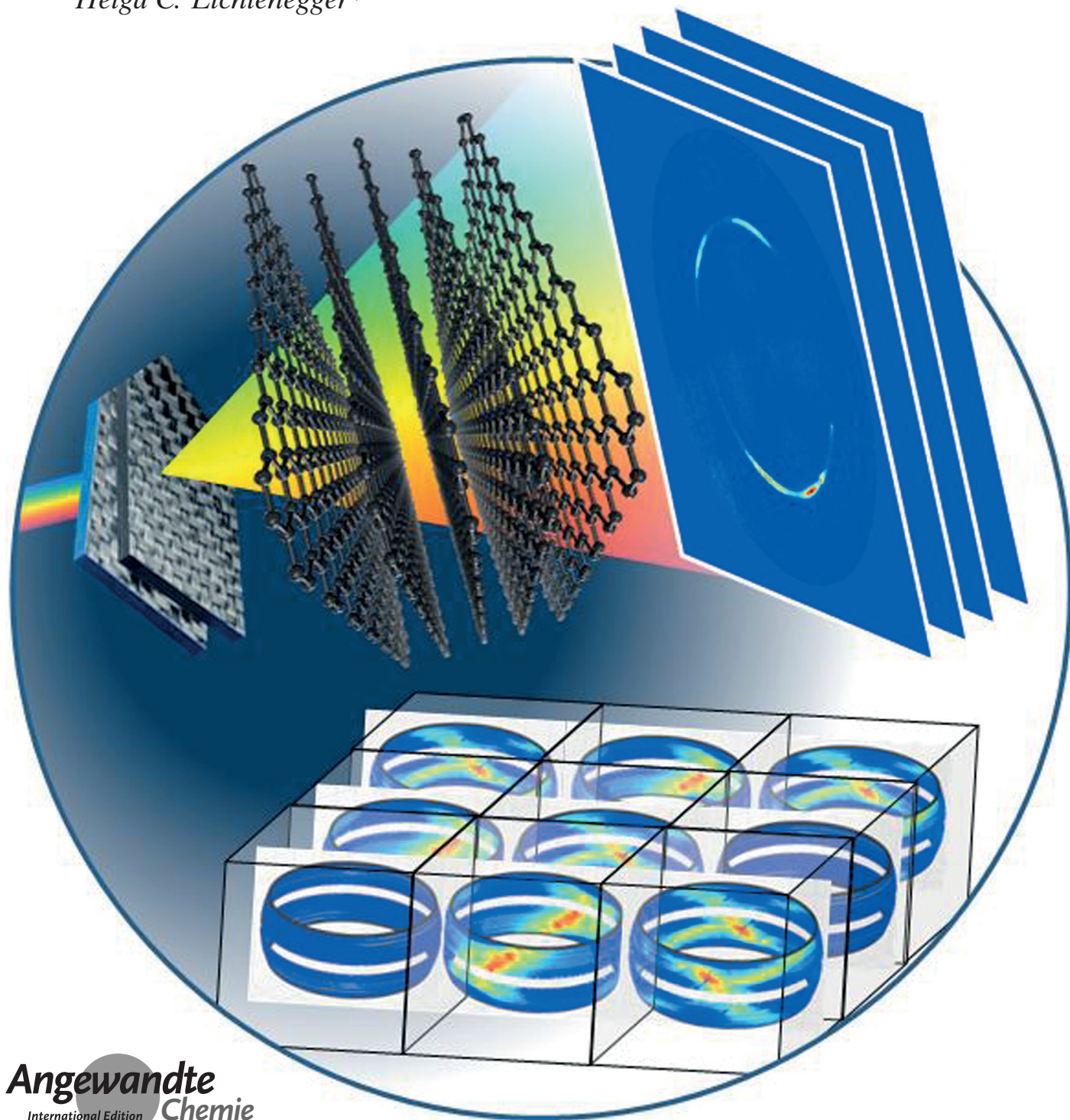


Crystallographic Texture

International Edition: DOI: 10.1002/anie.201603784
German Edition: DOI: 10.1002/ange.201603784

Photon Energy Becomes the Third Dimension in Crystallographic Texture Analysis

*Tilman A. Grünewald, Harald Rennhofer, Pieter Tack, Jan Garrevoet, Didier Wermeille, Paul Thompson, Wim Bras, Laszlo Vincze, and Helga C. Lichtenegger**



Abstract: Conventional analysis of the preferred orientation of crystallites (crystallographic texture) involves X-ray diffraction with area detectors and 2D data output. True 3D, spatially resolved information requires sample rotation in the beam, thus changing the probed volume, which introduces signal smearing and precludes the scanning of complex structures. This obstacle has been overcome by energy-dispersive Laue diffraction. A method has been devised to reach a large portion of reciprocal space and translate the X-ray photon energy into the missing third dimension of space. Carbon fibers and lobster exoskeleton as examples of biomineralized tissue have been analyzed. The major potential of this method lies in its “one-shot” nature and the direct 3D information requiring no previous knowledge of the sample. It allows the texture of large samples with complex substructures to be scanned and opens up the conceptual possibility of following texture changes *in situ*, for example, during crystallization.

X-ray diffraction (XRD) is a powerful method for the determination of the preferred orientation of crystallites (crystallographic texture). It relies on the sensitivity of the occurrence of X-ray reflections to the orientation of crystallographic planes. Crystallographic texture has a strong influence on the properties of materials^[1] and is also intimately linked with crystallization processes and reveals rare insights into crystal growth.^[2]

The development of large and sensitive X-ray area detectors has led to convenient measurement methods to simultaneously collect reflections at different angles and acquire 2D information. Nevertheless, this method lacks information about the third dimension. 3D information is achieved by sample rotation in the beam, which is feasible for small and homogeneous samples. In samples larger than the beam, the irradiated volume changes during rotation and different structural features contribute to the signal, thus

smearing the result. Under special conditions, X-ray diffraction can be exploited for tomographic determination of crystal orientation, as recently achieved for bone with small-angle X-ray scattering (SAXS)^[3] or for teeth with XRD.^[4] Tomographic methods, however, require rotation, considerable computing effort, and reach their limits in the case of very complex structures.

As a consequence of the sensitivity of the diffraction conditions to both crystallite orientation and incident energy, the diffraction of a white beam probes different crystal planes in the irradiated sample spot simultaneously. This approach is known as Laue diffraction, the oldest technique of single-crystal XRD,^[5] and has gained new momentum with the advent of high brilliance white synchrotron microbeams.^[6] It can be used for polycrystalline materials, as long as the beam size is sufficiently small to irradiate only a few grains so as to identify individual diffraction spots.^[7] Depth-profiling is also possible with 3D XRD approaches such as differential-aperture X-ray microscopy,^[1b] which requires time-consuming aperture scanning. Once the crystallite size falls much below the achievable beam size, such as in nanocrystalline materials, reflections from different crystallite orientations overlap and smear the scattering pattern—unless the different reflections can be separated by their respective energy. Attempts have been made in the past using energy-dispersive point detectors for texture measurement.^[8] A technological leap forward was the development of an energy-dispersive area detector (X-ray color camera, pnCCD)^[8,9] which, in principle, allows energy-dispersive Laue diffraction (EDLD). Despite it being a very small detector, it was successfully used, for example, for XRD of twinned lysozyme crystals^[10], strain measurements in a Cu single crystal,^[11] and the indexing of a GaAs single crystal with hard X-rays^[12], where the experiment required only a small angular coverage of reciprocal space.

Here we report on the first EDLD texture measurements using an energy-dispersive pnCCD camera (SLcam) and exploiting a wide range of scattering angles (i.e. a large portion of reciprocal space) as well as a reconstruction algorithm for 3D representation without a priori knowledge. The conventional 2D information available from area detectors is complemented by an energy spectrum recorded in each pixel, thus effectively using the energy to access the missing third dimension. 3D information can be acquired in a single shot, without sample rotation, and at a spatial resolution only limited by the beam size at a given sample thickness. The accessible 3D information is, however, limited by the usable energy window and accessible scattering angles. Therefore, the method is of particular value for experiments where full sample rotation is unsuitable—because of the complexity of the sample, for rapid 2D texture mapping, for following fast *in situ* processes, or for setups that do not allow rotation. The measurement scheme is depicted in Figure 1.

We used carbon fibers for a proof of principle: they can be prepared in a controlled orientation and exhibit a well-known fiber texture. Single carbon fibers can be visualized as consisting of graphene layers stacked at regular intervals to form graphite (Figure 2a), with the layers mainly parallel to the longitudinal axis and rotated randomly about it.^[13] In reciprocal space, every set of stacked graphene layers will

[*] Dr. T. A. Grünewald, Dr. H. Rennhofer, Prof. H. C. Lichtenegger

Institute of Physics and Materials Science
University of Natural Resources and Life Sciences (BOKU)
Peter Jordan Strasse 82, 1190 Vienna (Austria)
E-mail: helga.lichtenegger@boku.ac.at


P. Tack, Prof. L. Vincze
Department of Analytical Chemistry
Ghent University (Belgium)

Dr. J. Garrevoet
Deutsches Elektronen Synchrotron
Hamburg (Germany)

Dr. D. Wermeille, P. Thompson
XMaS—The UK CRG Beamline, ESRF—The European Synchrotron
Grenoble, Cedex 9 (France)

Dr. D. Wermeille, P. Thompson
Department of Physics
University of Liverpool (UK)

Dr. W. Bras
DUBBLE@ESRF, Netherlands Organisation for Scientific Research (NWO)
Grenoble Cedex 9 (France)

 Supporting information and the ORCID identification number(s) for the author(s) of this article can be found under <http://dx.doi.org/10.1002/anie.201603784>.

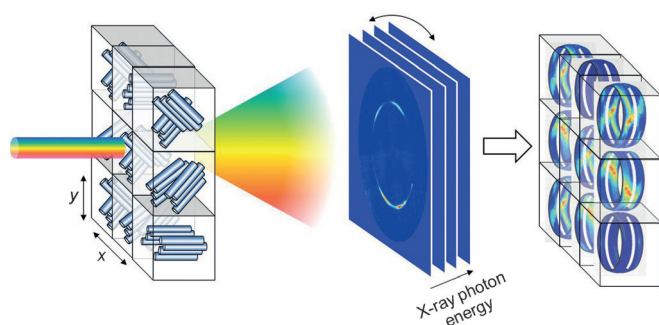


Figure 1. Energy-dispersive Laue diffraction for texture measurements. A crystalline sample slice with locally varying crystallite orientation (here: crystalline fibers) is scanned with a narrow white X-ray beam (visualized by a different X-ray “colors”). Diffraction patterns are recorded with an energy-dispersive area detector, and 3D orientation information at every pixel is immediately available from the stack of energy-dispersive diffraction images. The detector was also rotated to cover a wide range of scattering angles. The x - and y -axis are the coordinates of the sample slice. The third dimension in the resulting orientation map (right) is derived from the X-ray photon energy.

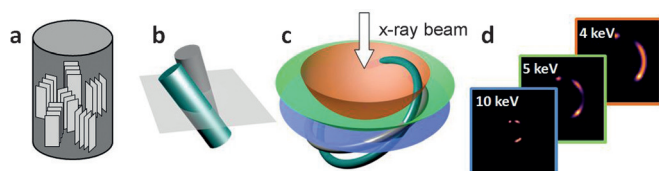


Figure 2. Diffraction from carbon fibers. a) Model of the fiber texture from rotational averaging of all crystallite orientations. b) Two inclined fibers in real space sticking out of the sample plane. c) The (002) reflection rings of graphite in reciprocal space and their intersection with Ewald spheres at different energies: 10 (blue), 5 (green), 4 keV (red). d) Simulated scattering patterns from two inclined fibers as shown in (b) at different energies.

yield one Bragg reflection from the graphite (002) planes, which is represented by a diffraction spot. Assuming perfect fiber texture, the spots will smear out to a ring perpendicular to the fiber axis. The same consideration holds for two or more fibers in different orientations (Figure 2b). If the fibers are tilted, the (002) rings are also tilted in reciprocal space (Figure 2c). Performing an XRD experiment is equivalent to intersecting the reflection rings with a sphere of radius $k = 2\pi/\lambda$ (Ewald sphere), where k is the wavenumber and λ the wavelength of the incident X-rays. Multiple photon energies correspond to multiple wavelengths ($E = hc/\lambda$; h is the Planck constant and c the speed of light) and are represented by multiple spheres with different radii (Figure 2c). For lower energies, the radius k decreases, that is, the curvature increases and the points of intersection shift along the reflection ring, thus yielding 3D information (Figure 2d).

In monochromatic XRD, the curvature of the Ewald sphere can be used to gain limited 3D information, as used for some biological applications.^[14] Real 3D information on an unknown texture, however, requires a wide range of energies. As a result of the pronounced curvature of the Ewald sphere at low energies, the low energy part of the spectrum contributes considerably to the 3D information and, accord-

ing to the Bragg equation $\lambda = 2d \cdot \sin\theta$, is associated with large diffraction angles 2θ at a given crystal-lattice spacing d .

One stringent requirement for the experiment is that a wide range of scattering angles must be covered. By using a very compact setup and detector rotation, we achieved 2θ values up to 40° , which proved sufficient for useful texture information. Diffraction images from carbon fibers were obtained by irradiation with a $40 \times 40 \mu\text{m}^2$ white beam from a bending magnet (XMaS, ESRF) and recorded by the energy-dispersive SLcam, where each pixel comprises an energy spectrum (Figure 3a). A Python program was used to obtain diffraction image stacks of different energies (Figure 3b). Considering the position of the diffracted intensity on the azimuth χ and the dependent scattering angle 2θ , the image stack can be transformed into 3D images (Figure 3c) and a pole figure can immediately be derived (Figure 3d).

The 3D diffraction image (Figure 3c) and the pole figure (Figure 3d) clearly show two inclined rings with an area of higher intensity where they intersect (Figure 3e). As these correspond to the (002) reflection of graphite in carbon fibers, the orientation of the carbon fiber in real space (Figure 3f) can be immediately seen. In monochromatic X-ray diffraction, only one individual image of Figure 3b would be obtained and the different orientations could not be extracted. Further examples are found in the Supporting Information.

The white spectrum of the incident X-rays also results in fluorescence being excited in the sample. This can, on the one hand, be regarded as an asset, since it gives immediate information on the elemental composition. On the other hand, fluorescence radiation is often stronger than the diffraction signal, thus making certain energies of the spectrum unusable for evaluation. As a consequence of the narrow width of the fluorescence signal and the good energy resolution of the detector (150 eV), this effect was limited in our experiment. It could become more severe when many elements with strong fluorescence signals close to each other and within the used energy range are present.

The most important limitation is given by the available energy window (here ca. 4.5–40 keV) and the corresponding scattering angles, which depend on the sample structure. Different ranges of scattering angles will occur for different reflections (different d -spacings). For example, for the graphite (002) reflection (d -spacing of $d_{002} = 0.335$ nm), the above energy range translates into scattering angles 2θ from 5 to 47° . Our setup covered measured angles 2θ from 5 to 40° and was, therefore, well-adapted to the sample system. In the pole figures we correspondingly covered a latitude range from 2.5 to 20° . It should be noted that any signal falling exclusively into the white spots in the pole figure will not be detected. For example, carbon fibers oriented parallel to the beam will give no detectable signal, because the reflection ring will lie in the white region at the equator of the pole figure. Blind spots can be largely avoided in texture measurements with full sample rotation, but still occur around the rotation axis. They can be covered by rotation about a second axis. To be meaningful, this requires sufficient homogeneity of the sample and a suitable experimental setup. These conditions are frequently not fulfilled.

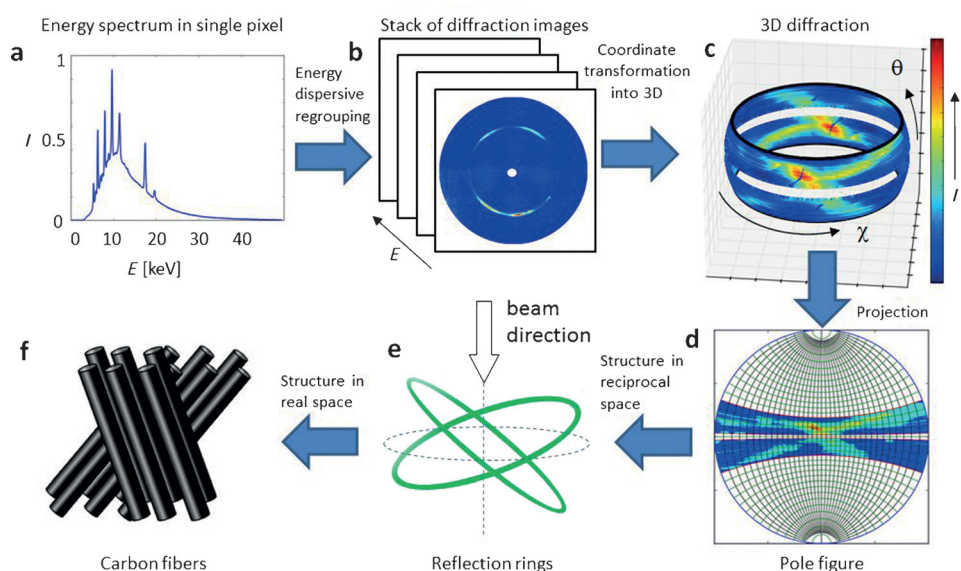


Figure 3. Data processing. a) Energy spectrum in one SLcam pixel. b) Scattering image stack: energy from 1 to 40 keV. The white spot in the center is the beamstop. c) 3D diffraction image. The longitude is given by the azimuth χ and the latitude by the half diffraction angle θ . The white stripe at the equator corresponds to diffraction angles blocked by the beamstop. The maximum latitude is given by the maximum diffraction angle. d) Projection of the 3D image in a pole figure. e) 3D texture in reciprocal space: crossed rings of (002) reflections. f) Carbon fiber orientation in real space.

Since our approach also yields direct 3D information in a nonrotational setup, it is particularly suited for texture scanning of hierarchically structured, complex materials and can also be used effectively to clarify unknown textures within the limitations described above. Biomineralized tissues, such as bone, teeth or crustacean cuticle, are known to exhibit intricate patterns of crystallite orientation.^[4,15]

The cuticle of American lobster (*Homarus americanus*) consists of layers of helicoidally arranged chitin fibers (Figure 4a) mineralized mainly with amorphous calcium carbonate. Crystalline calcite is reported to occur in the exocuticle, with the crystal *c*-axis oriented roughly perpendicular to the chitin layer.^[16] Since the calcite (104) reflection occurs at an angle of about 45° versus the *c*-axis, a fiber texture would yield a ring in reciprocal space (Figure 4b). EDLD texture measurements were performed on 10 μm thick slices of the tail cuticle. The 3D diffraction representation (Figure 4c) shows fractions of a (104) ring, consistent with a *c*-axis orientation slightly tilted versus the layer normal.^[15] The spotty signal instead of a smooth ring indicates large crystals with a preferred orientation rather than small crystallites with fiber texture (Figure 4d). The measurement of additional points in the lobster endocuticle yielded Ca fluorescence, but no crystalline calcite. This is compatible with the literature, where amorphous CaCO_3 was reported for the endocuticle.^[16]

We have shown that EDLD texture measurements are a unique 3D analysis tool that yields “one-shot” pole figures, with a spatial resolution limited only by the beam size at a given sample thickness. In our experiment, acquisition times were still several minutes per position, but this can be shortened considerably by beam focusing and, preferably, a faster detector read-out. The advent of bright laboratory sources makes this setup also feasible in a laboratory setting.

A further extended range of diffraction angles will yield a larger portion of reciprocal space. This could be achieved by larger and preferably bent detector chips to limit parallax. The energy-dispersive/multiwavelength approach gives simultaneous diffraction and X-ray fluorescence signals in the SLcam (fluorescence lines in Figure 2a), thereby delivering structural and element information at the same time. The greatest advantage of this new method is the 3D information inherently available within the used energy window, at good time and spatial resolution. It is suitable for fast sample mapping and makes the study of correlated effects, for example, crystallization and strain development, conceivable. As such, it has the potential to effectively replace a considerable

fraction of both traditional Laue diffraction and monochromatic diffraction, and become an important tool in applied chemistry and materials science.

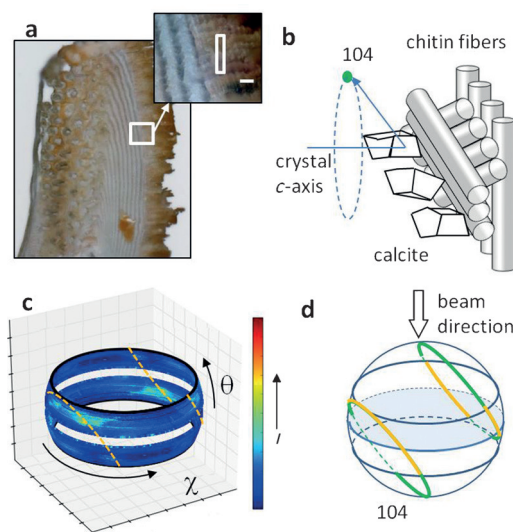


Figure 4. Texture of lobster cuticle. a) Micrograph of a thin section of lobster cuticle, showing the lamellar structure of the exoskeleton. The investigated region is marked with a white rectangle. Scale bar: 20 μm . b) Model of chitin layers and calcite crystallites. If the (104) reflection exhibits a fiber texture, it will be smeared into a ring perpendicular to the *c*-axis. The calcite crystallites are drawn here as randomly shaped particles, because the method is not supposed to give information on crystallite morphology. c) Experimental 3D diffraction of calcite (104). Dashed lines correspond to likely orientations of the diffraction rings. d) Orientation of (104) diffraction rings measured in (c). The yellow fractions of the ring correspond to visible portions within the experimental limits.

Experimental Section

The experiments were performed at the UK CRG beamline XMaS, BM28 at the European Synchrotron Radiation Facility (ESRF), Grenoble, France. A white X-ray beam from a bending magnet was shaped by a slit collimation system to a final size of $40 \times 40 \mu\text{m}^2$. The scattered radiation was recorded in a transmission setup with an energy-dispersive 2D detector (SLcam) mounted on a 6-circle Huber diffractometer. The detector was scanned in a 4×4 array to cover a larger angular space. The data were processed in home-written Python programs. Background subtraction was carried out by exploiting the energy spectrum in every pixel of the detector. A q -region without a Bragg reflection was used and the intensity of the background signal was normalized to that of the sample. Although being a phenomenological approach, it worked very well for our samples with little amorphous background and sufficient transmission. The transmission factor at the lowest energy (4.5 keV) was 0.69 and 0.94 for lobster cuticle and carbon fibers, respectively. Further details can be found in the Supporting Information.

Acknowledgements

We thank Andrea Scheberl (Department of Nanobiotechnology, BOKU Vienna, Austria) and Hiram Castillo (ESRF, ID21, Grenoble, France) for cutting samples. Carbon fibers and advice were provided by Herwig Peterlik (Institute of Materials Physics, University of Vienna, Austria). We thank Daniel Irrasch, Tobias Steurer, and Reinhard Schuller (Department of Materials Sciences and Process Engineering, BOKU Vienna, Austria) for mechanical engineering. Financial support was provided by the Berndorf Privatstiftung, Vienna. P.T. was funded through a PhD grant from the Agency for Innovation by Science and Technology (IWT). XMaS is a UK midrange facility supported by the EPSRC. We thank The European Synchrotron (ESRF) for making beam time available, and the XMaS and DUBBLE staff for their support. We thank J. Kieffer for support with the PyFAI software package. We thank D. Pontoni (ESRF) for initiating and supporting the scientific collaboration that led to this work. We acknowledge the Partnership for Soft Condensed Matter (PSCM) established by the ESRF and the ILL at the European Photon and Neutron (EPN) Science Campus Grenoble for providing a fruitful scientific environment. The frontispiece contains the image “isolated graphite” © Owen Thomas | Dreamstime.com.

Keywords: biomineralization · crystallographic texture · energy-dispersive Laue diffraction · X-ray diffraction

How to cite: *Angew. Chem. Int. Ed.* **2016**, *55*, 12190–12194
Angew. Chem. **2016**, *128*, 12376–12381

- [1] a) P. Bleuet, E. Welcomme, E. Dooryhee, J. Susini, J. L. Hodeau, P. Walter, *Nat. Mater.* **2008**, *7*, 468–472; b) B. C. Larson, W. Yang, G. E. Ice, J. D. Budai, J. Z. Tischler, *Nature* **2002**, *415*, 887–890; c) J. Huber, E. Griesshaber, F. Nindiyasari, W. W. Schmahl, A. Ziegler, *J. Struct. Biol.* **2015**, *190*, 173–191.
- [2] I. C. Olson, R. Kozdon, J. W. Valley, P. U. P. A. Gilbert, *J. Am. Chem. Soc.* **2012**, *134*, 7351–7358.
- [3] a) F. Schaff, M. Bech, P. Zaslansky, C. Jud, M. Liebi, M. Guizar-Sicairos, F. Pfeiffer, *Nature* **2015**, *527*, 353–356; b) M. Liebi, M. Georgiadis, A. Menzel, P. Schneider, J. Kohlbrecher, O. Bunk, M. Guizar-Sicairos, *Nature* **2015**, *527*, 349–352.
- [4] C. K. Egan, S. D. Jacques, M. Di Michiel, B. Cai, M. W. Zandbergen, P. D. Lee, A. M. Beale, R. J. Cernik, *Acta Biomater.* **2013**, *9*, 8337–8345.
- [5] a) C. Detavernier, A. S. Ozcan, J. Jordan-Sweet, E. A. Stach, J. Tersoff, F. M. Ross, C. Lavoie, *Nature* **2003**, *426*, 641–645; b) N. Tamura, P. U. P. A. Gilbert in *Research Methods in Biomineralization Science*, Vol. 532 (Ed.: J. J. D. Yoreo), **2013**, pp. 501–531; c) B. D. Cullity, *Elements of x-ray diffraction*, 2nd ed., Addison-Wesley, Reading, Massachusetts, **1978**.
- [6] D. F. Sanchez, J. Villanova, J. Laurencin, J.-S. Micha, A. Montani, P. Gergaud, P. Bleuet, *J. Appl. Crystallogr.* **2015**, *48*, 357–364.
- [7] a) I. C. Olson, R. A. Metzler, N. Tamura, M. Kunz, C. E. Killian, P. U. Gilbert, *J. Struct. Biol.* **2013**, *183*, 180–190; b) J. D. Budai, W. G. Yang, N. Tamura, J. S. Chung, J. Z. Tischler, B. C. Larson, G. E. Ice, C. Park, D. P. Norton, *Nat. Mater.* **2003**, *2*, 487–492.
- [8] a) C. Genzel, I. A. Denks, R. Coelho, D. Thomas, R. Mainz, D. Apel, M. Klaus, *J. Strain Anal. Eng. Des.* **2011**, *46*, 615–625; b) M. Wehrhahn, R. A. Schwarzer, *Z. Metallkd.* **1994**, *85*, 581–584.
- [9] a) I. Ordavo, et al. *Nucl. Instrum. Methods Phys. Res. Sect. A* **2011**, *654*, 250–257; b) O. Scharf, et al., *Anal. Chem.* **2011**, *83*, 2532–2538; c) S. Send, et al., *J. Appl. Crystallogr.* **2009**, *42*, 1139–1146; d) W. Leitenberger, R. Hartmann, U. Pietsch, R. Andritschke, I. Starke, L. Struder, *J. Synchrotron Radiat.* **2008**, *15*, 449–457.
- [10] S. Send, A. Abboud, W. Leitenberger, M. S. Weiss, R. Hartmann, L. Strüder, U. Pietsch, *J. Appl. Crystallogr.* **2012**, *45*, 517–522.
- [11] A. Abboud, C. Kirchlechner, S. Send, J. S. Micha, O. Ulrich, N. Pashniak, L. Strueder, J. Keckes, U. Pietsch, *Rev. Sci. Instrum.* **2014**, *85*, 113901.
- [12] S. Send et al., *J. Appl. Crystallogr.* **2016**, *49*, 222–233.
- [13] O. Paris, D. Loidl, H. Peterlik, *Carbon* **2002**, *40*, 551–555.
- [14] a) H. Lichtenegger, M. Müller, O. Paris, C. Riekel, P. Fratzl, *J. Appl. Crystallogr.* **1999**, *32*, 1127–1133; b) O. Paris, M. Müller, *Nucl. Instrum. Methods Phys. Res. Sect. B* **2003**, *200*, 390–396; c) M. Ogurreck, H. C. Lichtenegger, M. Müller, *J. Appl. Crystallogr.* **2010**, *43*, 256–263; d) M. Erko, et al., *J. R. Soc. Interface* **2015**, *12*, 20141111.
- [15] a) W. Wagermaier, H. S. Gupta, A. Gourrier, O. Paris, P. Roschger, M. Burghammer, C. Riekel, P. Fratzl, *J. Appl. Crystallogr.* **2007**, *40*, 115–120; b) S. Schrof, P. Varga, L. Galvis, K. Raum, A. Masic, *J. Struct. Biol.* **2014**, *187*, 266–275; c) H. C. Lichtenegger, T. Schöberl, M. H. Bartl, J. H. Waite, G. D. Stucky, *Science* **2002**, *298*, 389–392; d) T. A. Grünwald, H. Rennhofer, B. Hesse, M. Burghammer, S. Stanzl-Tschegg, M. Cotte, J. F. Löffler, A. M. Weinberg, H. C. Lichtenegger, *Biomaterials* **2016**, *76*, 250–260.
- [16] A. Al-Sawalmih, C. Li, S. Siegel, H. Fabritius, S. Yi, D. Raabe, P. Fratzl, O. Paris, *Adv. Funct. Mater.* **2008**, *18*, 3307–3314.

Received: April 19, 2016

Revised: May 31, 2016

Published online: August 2, 2016